Opto-Electronic Advances

Review

2018, Vol. 1, No. 10

DOI: 10.29026/oea.2018.180021

Nonlinear frequency conversion in optical nanoantennas and metasurfaces: materials evolution and fabrication

Mohsen Rahmani[1]*, Giuseppe Leo[2], Igal Brener[3], Anatoly V. Zayats[4], Stefan A. Maier[5,6], Costantino De Angelis[7], Hoe Tan[1], Valerio Flavio Gili[2], Fouad Karouta[1], Rupert Oulton[5], Kaushal Vora[1], Mykhaylo Lysevych[1], Isabelle Staude[8], Lei Xu[9], Andrey E. Miroshnichenko[9], Chennupati Jagadish[1] and Dragomir N. Neshev[1]

Nonlinear frequency conversion is one of the most fundamental processes in nonlinear optics. It has a wide range of applications in our daily lives, including novel light sources, sensing, and information processing. It is usually assumed that nonlinear frequency conversion requires large crystals that gradually accumulate a strong effect. However, the large size of nonlinear crystals is not compatible with the miniaturisation of modern photonic and optoelectronic systems. Therefore, shrinking the nonlinear structures down to the nanoscale, while keeping favourable conversion efficiencies, is of great importance for future photonics applications. In the last decade, researchers have studied the strategies for enhancing the nonlinear efficiencies at the nanoscale, e.g. by employing different nonlinear materials, resonant couplings and hybridization techniques. In this paper, we provide a compact review of the nanomaterials-based efforts, ranging from metal to dielectric and semiconductor nanostructures, including their relevant nanofabrication techniques.

Keywords: nonlinear nanophotonics; metallic nanoantennas; dielectric nanoantennas; III-V semiconductor nanoantenna; nanofabrication

Rahmani M, Leo G, Brener I, Zayats A V, Maier S A, *et al*. Nonlinear frequency conversion in optical nanoantennas and metasurfaces: materials evolution and fabrication. *Opto-Electronic Advances* **1**, 180021 (2018).

Introduction

Advanced nanofabrication techniques have enabled complicated assemblies of nanoscale structures that can be employed for engineering the electromagnetic behaviour at optical frequencies. Nanophotonics, i.e. the technology of generating, controlling, and detecting photons, via engineered nanostructures, is considered to be a revolutionary technology for the 21st Century[1]. The field of intense light interaction with nanostructures, so called nonlinear nanophotonics, is one of the most attractive branches of nanophotonics that studies multifrequencies interactions in nanoscale devices, including the distribution and guiding the generated frequencies in selected

[1]Research School of Physics and Engineering, The Australian National University, Canberra ACT 2601, Australia; [2]Matériaux et Phénomènes Quantiques, Université Paris Diderot-Sorbonne Paris Cité, 10 rue A. Domon et L. Duquet, 75013 Paris, France; [3]Center for Integrated Nanotechnologies, Sandia National Laboratories, Albuquerque, New Mexico 87185, United States; [4]Department of Physics, King's College London, Strand, London WC2R 2LS, United Kingdom; [5]The Blackett Laboratory, Department of Physics, Imperial College London, London, SW7 2AZ, United Kingdom; [6]Chair in Hybrid Nanosystems, Nano Institute Munich, Fakultät für Physik, Ludwig-Maximilians-Universität München, München, Germany; [7]Deptartment of Information Engineering, Universitàdegli Studi di Brescia and INO-CNR, Via Branze 38, 25123 Brescia, Italy; [8]Institute of Applied Physics, Abbe Center of Photonics, Friedrich Schiller University Jena, 07745 Jena, Germany; [9]School of Engineering and Information Technology, University of New South Wales, Canberra ACT 2600, Australia

* Correspondence: M Rahmani, E-mail: mohsen.rahmani@anu.edu.au

Received 21 October 2018; accepted 13 November 2018; accepted article preview online 7 December 2018

frequency ranges. This field plays an important role in modern photonic devices, including optical signal processing, control over the frequency spectrum of laser light, ultrafast switching and generation of ultrashort pulses[2,3].

The nonlinear optical response of nanostructured materials is generally very weak. However, recent studies have revealed the potential of nanophotonics to address this issue via artificially induced nonlinear responses in optically resonant nanostructures[3–15]. This is possible, since metallic and dielectric nanostructures are capable of squeezing light fields into volumes much smaller than the diffraction limit. In other words, nanostructures can act as optical antennas thus reversibly transferring propagating electromagnetic waves into volumes orders of magnitude smaller than the diffraction limit of light[16–18]. Such concentration of the optical fields to nanoscale volumes strongly promotes and enhances nonlinear effects at the nanoscale. In particular, nonlinear frequency conversion at the nanoscale can result in novel nanoscale light sources, including sources of single quanta of light. Such sources will advance the performance, energy efficiency and security of future optical communication networks and computing systems. However, the fabrication of nonlinear nanoantennas and their functionalities requires novel approaches and materials to efficiently convert optical fields from one frequency to another. Importantly, the chosen materials should be resistant enough against heat generated by high-power lasers, and preferably exhibit minimal optical losses.

Here, we review the materials evolution and various approaches for fabricating nanostructured materials for nonlinear frequency conversion. We provide detailed analysis of both advantages and disadvantages of each material, in terms of nonlinear properties, nanofabrication and explain why research interests have migrated from one material to another. Notably, the comparison between nonlinear efficiencies and characteristics of nanoantennas, that are already well-reviewed[19–22], are beyond the scope of this review paper. This exception includes the factors that can enhance the conversion efficiency but are not necessarily related to the material of antennas, such as mode compositions in the fundamental and/or harmonic generation wavelengths, various types of couplings and various types of mode interferences, etc[19–22].

Metallic nanoantennas

Metals were among the first exploited nanoscale materials to obtain strong optical nonlinear responses[5–11,18–25]. Metallic nanostructures represent an interesting approach to bridge the gap between conventional and modern optics. Such nanostructures stimulate the oscillation of free electrons on the surface, so-called surface plasmons[5–11,18–23,26–32] that lead to strong near-field enhancements known as hot-spots that boost both linear and nonlinear characteristics[9,33–38]. Indeed, employing surface plasmons arising at metal-dielectric boundaries allows enhancing nonlinear interactions, because electrons at the surface reside in a non-symmetric environment, where the nonlinearities arise from the asymmetry of the potential confining the electrons at the surface[2,3]. Moreover, additional degrees of freedom, e.g. couplings between the constituent nanoparticles, suggest a departure from conventional physical limitations in nonlinear optics. For instance, Gennaro et al. have recently shown that multi-resonant nanoantennas reveal the interplay of symmetry and scattering phase that directly influences Second Harmonic Generation (SHG)[39], which is a coherent nonlinear process that converts two photons of frequency ω into one photon of frequency 2ω[9]. Figure 1(a) shows how two disks (2ω-particles) in the nanoantenna on the left radiate in phase leading to bright and directional SHG, while SHG is suppressed as its 2ω-particles radiate out of phase. The SEM images of the fabricated plasmonic structures and the experimental results of the SHG are plotted in Figs. 1(b) and 1(c), respectively.

Fabrication of metallic nanoantennas is relatively straight forward by using electron beam lithography

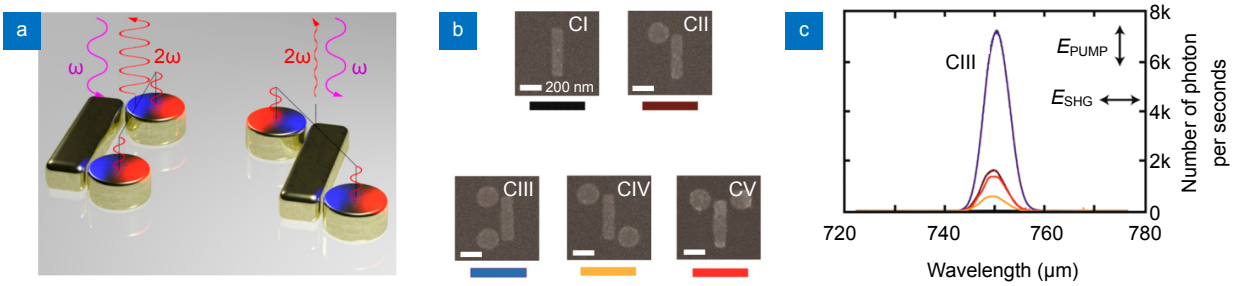

Fig. 1 | (**a**) An illustration of SHG interference in multi-resonant gold nanoantennas. (**b**) SEM images of the five nanoantennas configuration (CI−CV). Dimensions of the bars are 340 nm×80 nm×40 nm in *x*, *y*, and *z*, respectively, while disks are the same thickness with diameters of 160 nm. The gaps between the disks and the bar are 20 nm for all cases. (**c**) The measured SHG signals from the five configurations, where the pump and SHG signal are polarized along and perpendicular to the bar, respectively. The colors of various curves correspond to different antennas, shown in (b). Figure reprinted with permission from ref.[9], American Chemical Society.

(EBL). Since metal films can be deposited by electron beam/thermal evaporation or sputtering, both at room temperature, the thin metal film deposition process does not damage the electron beam resist. Therefore, high quality nanoantennas, patterned by an electron beam on the resist, can be transferred to the metal films by a lift-off technique, leading with minimal variations.

Another plasmonic structure important for the enhancement of the nonlinear effects is the gold nanorod metamaterial slabs, so called hyperbolic metamaterial (see Fig. 2(a)), providing unusual linear and nonlinear optical properties[40–42]. Such Au nanorods are electrochemically grown in a substrate-supported, porous, anodized aluminium oxide (AAO) template[43]. The substrate is a multi-layered structure comprising a glass substrate, a few nanometer-thick Ta_2O_5 base adhesion layer, and a few nanometer Au film acting as the working electrode for the electrochemical reaction. A thick aluminium film, around half a micrometre, is then deposited via planar magnetron sputtering onto the electrode. This Al film is subsequently anodized in sulphuric acid, producing the porous AAO template, followed by the electrochemical growth of the nanorods and finally removing AAO template[43]. This fabrication technique leads to the generation of nanorods with ~10 nm diameter (see Fig. 2(a)) that can increase the intensity of far-field SHG by three orders of magnitude compared to the uniform dielectric. The enhancement is related to both the local field enhancement in the metamaterial and its ability to convert dark evanescent SH field components generated by the nanoparticle into radiative modes, detectable in the far-field. A comparison with the metamaterial SHG intensities for TE and TM excitations at an angle of incidence of 60° shows that the gold nanorod metamaterial outperforms the Au film in the resonant conditions by approximately two orders of magnitude (see Fig. 2(b)).

Group IV semiconductor nanoantennas

Despite numerous advantages allowing for near-field enhancement, metallic nanostructures suffer from ohmic losses at optical frequencies, which limit their functionalities. Because of the ohmic losses, metals tend to absorb light and get heated remarkably. Hence metallic nanostructures can be irreversibly damaged under illumination by high power lasers. Therefore, the exploration of other materials for nonlinear enhancement at the nanoscale has recently been an active research direction[44–68]. High-refractive index resonant nanoparticles, e.g. silicon[44] and germanium[45], with very low losses in visible and IR can offer new avenues to the study of nonlinear effects. They are emerging as promising alternatives to metallic nanoparticles for a wide range of nanophotonic applications that utilize localized resonant modes.

Furthermore, nanostructures with large refractive indices exhibit multipolar characteristics, supporting both electric and magnetic resonant optical modes[69]. The nonlinear optical effects are significantly enhanced at the optical resonances. In particular, the nonlinear optical effects are especially enhanced at the position of magnetic dipolar resonances as well as at the spectral position of the anapole mode, which is an interference of the electric dipole and toroidal modes[44]. Furthermore, when both electric and magnetic origins are present, the nonlinear response can be modified by magneto-electric coupling[70]. A detailed explanation of electric and magnetic modes and their interferences is beyond the scope of this review.

Another important advantage of high refractive index nanostructures is their large intrinsic nonlinear properties, i.e. second and third order susceptibilities. Silicon and germanium are centrosymmetric materials lacking second-order susceptibility, however they possess large third-order nonlinearity. As such, silicon and germanium nanostructures hold great promise for strong enhancement of the nonlinear optical response. The fabrication process for germanium nanoantennas is very similar to metals, as germanium can be deposited with standard evaporation techniques. Recently, Grinblat et al.[45] employed this technique for fabrication of germanium antennas on borosilicate glass. Using such germanium nanoantennas, they obtained efficient Third Harmonic Generation (THG), 100 times larger than the THG from an unstructured germanium film (Fig.3(a)). THG is a nonlinear interaction when three photons are combined

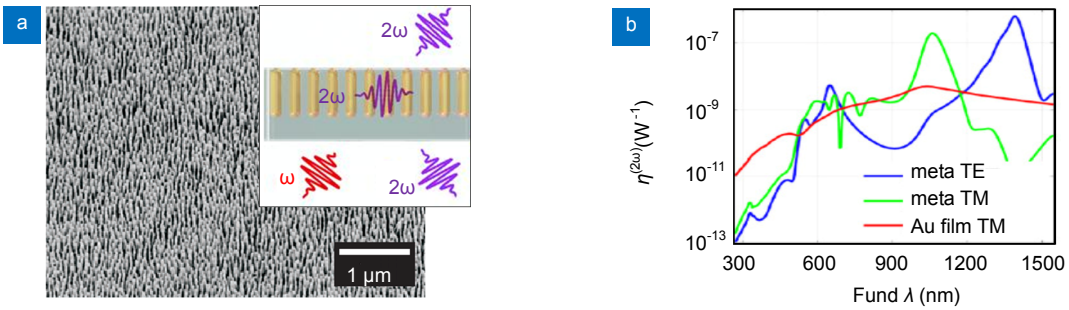

Fig. 2 | (**a**) Angled SEM view of metamaterial showing Au nanorods. Inset demonstrates the propagation of fundamental and SHG waves. (**b**) Far-field reflected SH spectra from a smooth Au surface (red line) and the nanorod metamaterial. Figure reproduced with permission from ref.[41], John Wiley and Sons.

to create a single photon at three times the frequency. The authors have engineered germanium nanostructures to maximize the inner electric energy at the desired excitation wavelength by excitation of an electric anapole mode. The measured third harmonic shows a well pronounced cubic dependence with a slight saturation at high input intensities (see Fig. 3), overall demonstrating high third harmonic upconversion efficiency.

Another heavily studied, high-refractive index material is silicon. Crystalline silicon films cannot be deposited through evaporation or sputtering. However, fabricating silicon film on insulators, so called SoI technology, is well established in the market of electronic devices[71]. Beyond electronics, SoI wafers have been significantly employed in optics, as well. SoI is the enabling platform for silicon photonics, where planar waveguides that strongly confines light are possible thanks to the high refractive index contrast between silicon core and a SiO_2 substrate. In the last few years, several groups have also used SoI wafers to fabricate nanoscale resonators[47] that can be used to stimulate nonlinear interaction at the nanoscale[46].

The general nanofabrication method via SoI substrates is to generate a set of masks on the top of the wafers by electron beam lithography, laser interference lithography[72,73], etc., followed by transferring the mask geometries into the silicon layer via inductively coupled plasma (ICP) etching. The last step is the removal of the mask via wet or dry etching[47,74]. Recently, Shcherbakov et al. demonstrated that by engineering the resonant modes of silicon nanoparticles, one could control the locally enhanced electromagnetic fields, giving rise to up to two orders of magnitude enhancement of the THG with respect to bulk silicon[72]. As can be seen in Fig. 4(b), the THG again follows a cubic power dependence and at high input intensities, the third harmonic radiation is bright enough to be observed by the naked eye[44,72,75].

More recently, amorphous silicon has also been employed as a dielectric material with a large third-order

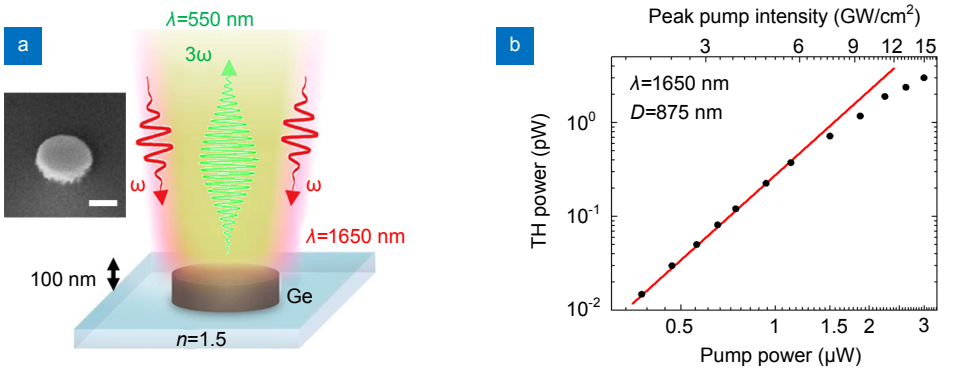

Fig. 3 | (**a**) Illustration of the THG process for a 100 nm thick germanium nanodisk on glass excited with near-infrared light of frequency ω to produce green emission of frequency 3ω. The inset shows SEM image of a germanium disk. Scale bar is 1 μm. (**b**) Measured TH power versus pump power at the AM (λ_{laser}=1650 nm, D=875 nm). The straight line is a fit considering the cubic dependence of the emission intensity on the excitation power. A deviation from this trend is observed from 1.5 μW. Figure reprinted with permission from ref.[45], American Chemical Society.

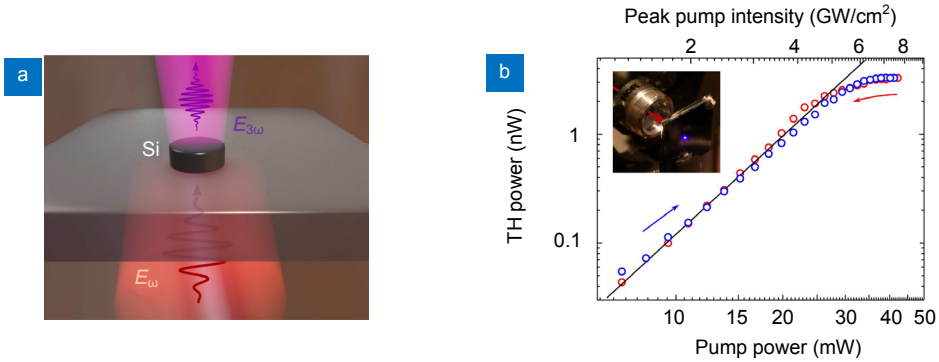

Fig. 4 | (**a**) Illustration of THG from individual Si nanodisks at optical frequencies. (**b**) Power dependence and conversion efficiency of the resonant THG process in Si nanodisks. Blue circles denote the THG power dependence upon increasing the power of the pump, while red circles denote the reverse procedure both obtained at λ=1260 nm fundamental wavelength. The inset shows a photographic image of the sample irradiated with the invisible IR beam impinging from the back side of the sample as indicated by the red arrow. The blue point represents the scattered TH signal detected by the camera. Figure reprinted with permission from ref.[72], American Chemical Society.

nonlinearity[48,49] and fast carrier recombination times[50,51]. Thin films of hydrogenated amorphous silicon are generally grown on a substrate by plasma enhanced chemical vapour deposition (PECVD). This tackles the limitation of SoI technology, i.e. fabricating of silicon nanoantennas on a fully transparent substrate, e.g. SiO_2 only. On the other hand, PECVD allows growing silicon films on any substrate that can be followed by ICP/RIE etching for nanofabrication. Recently, Xu et al, have demonstrated dielectric resonators on a metallic mirror (Fig. 5(a)) that can significantly enhance the third harmonic emission, as compared to a typical resonator on an insulator substrate[76]. As shown in Fig. 5(b), by employing a gold mirror under the silicon nanodisk promotes the resonantly excited anapole modes of the structures. This leads to a significant near-field enhancement that facilitates the nonlinear frequency conversion and results in record higher THG conversion efficiencies, as seen in Fig. 5(c). Therefore, the mirror surface boosts the nonlinear emission via the free charge oscillations within the interface, equivalent to producing a mirror image of the nonlinear source and the pump beneath the interface.

Group III-V semiconductor nanoantennas

The caveat of dielectrics, e.g. germanium and silicon, is their considerably weak intrinsic nonlinear second order susceptibility, where the centrosymmetric nature of these materials voids the second harmonic generation (SHG). The crystal symmetry of the excited structure has to be non-centrosymmetric in order to produce a nonzero SHG signal from the bulk of the material, as the SHG is a second-order nonlinear process. Therefore, silicon, germanium and other elemental semiconductors are not suitable for SHG. On the other hand, III-V semiconductors are non-centrosymmetric materials and benefit from large second-order susceptibilities[48,49,77] and fast carrier recombination times[50–52]. The strong second-order bulk susceptibility of III-V materials would therefore intrinsically increase the nonlinear conversion efficiency, as compared to silicon or germanium. Furthermore, like IV semiconductors, III-V semiconductors also exhibit high refractive indices that allow employing strong Mie-resonances[45,78–80] to boost the nonlinear signals. Subsequently, free standing III-V nanoantennas have been theoretically predicted to enhance the SHG efficiencies, significantly[53].

Unfortunately, the fabrication of III-V semiconductors on transparent substrates has not come to full fruition because of the absence of good quality dielectric-semiconductor interfaces. III-V semiconductors must be grown on a substrate with a minimal lattice mismatch to avoid defects. Recently, Cambiasso et al. have proposed an alternative to this issue. Instead of growing an III-V film for fabricating nanoantennas, they immediately made nanoantennas on the same wafer. They fabricated different designs of GaP nanoantennas of 200 nm height (Fig. 6(a)) by masking a GaP wafer using an EBL, followed by an ICP etching step[54]. The lossless GaP nanopillars are chosen for visible light applications.

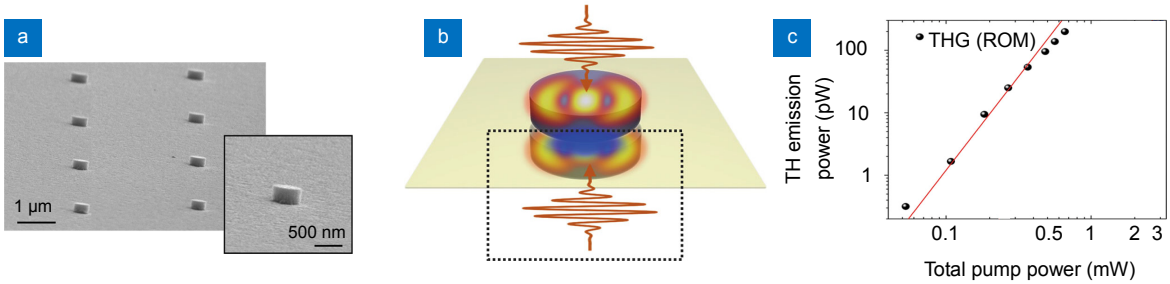

Fig. 5 | (**a**) SEM image of the fabricated resonator on mirror configuration. (**b**) Illustration of the current and field distributions of a resonator on a PEC substrate, respectively. (**c**) Measured TH power as a function of pump power. Figure reproduced from ref.[76].

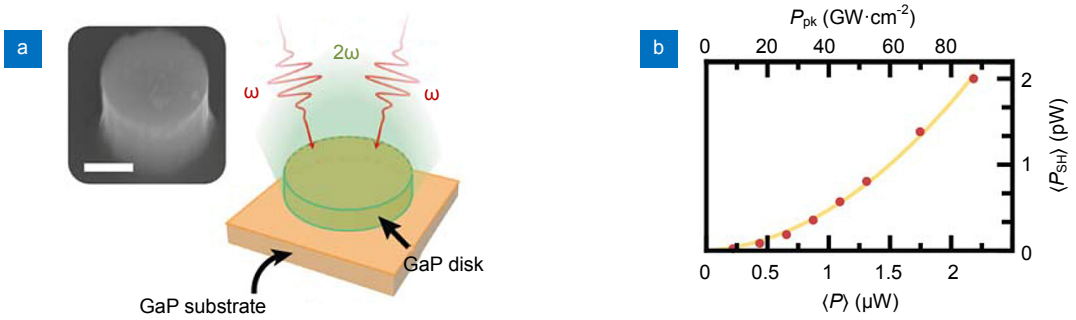

Fig. 6 | (**a**) SEM image of a 200 nm radius disk (scale bar is 200 nm), and a schematic view of the experimental setup for a disk emitting green SH light. (**b**) Dependence of the average SH power ⟨P_{SH}⟩ on the average excitation power ⟨P⟩ for the ND (corresponding pulse peak power ⟨P_{pk}⟩ on top axis). The solid line is a fit of the data considering the expected quadratic dependence of ⟨P_{SH}⟩ with ⟨P⟩. Figure reprinted with permission from ref.[54], American Chemical Society.

The authors have shown that the manipulation of resonant modes at the surfaces of the dielectric structure can benefit the nonlinear SHG characteristics for a single nanostructure, in the visible range with a good conversion efficiency (see Fig. 6(b)).

It is well-known that confined electromagnetic fields inside the resonators can be significantly enhanced if a large refractive index contrast between the resonators and the substrate is present. Therefore, more efficient nonlinear optical signals can be generated if high-refractive index nanoparticles are placed on oxide layers with low refractive indices. Indeed, the lack of a viable technology to produce high quality interfaces has been a barrier for reliable investigations and comprehensive understanding of compound semiconductor dielectric nanoantennas until very recently. GaAs nanoantennas have been recently fabricated on a glass substrate by Person et al.[55]. They implemented an epitaxial lift-off technique in conjunction with a water-bonding procedure to attach GaAs membrane (grown on a GaAs substrate) to a fused silica substrate. Using molecular beam epitaxy (MBE), a sacrificial layer of AlAs was grown on a GaAs substrate. On top of the AlAs layer a 1 μm film of GaAs was grown. Using the epitaxial lift-off procedure, the 1 μm GaAs film was transferred to a fused silica substrate. The transferred GaAs film was initially reduced to a thickness of ~150 nm by reactive ion etching (RIE). Disks were then patterned by EBL, followed by RIE. To this time, the authors only studied the forward and backward scattering from GaAs nanoparticles in the linear regime and did not explore the potential for nonlinear optics using such III-V structures on a transparent substrate.

Although, the abovementioned technique was the first of its kind, the low quality of resonators and the rough side-walls precluded to employing such nanopillars for applications in the nonlinear regime. Until recently, the full development of an III-V platform was hindered by the difficulty of fabricating monolithic shallow resonators in a way similar to the SoI platform. In particular, such opportunity was hindered by the shortcomings of wet selective oxidation of the epitaxial layers. To overcome these limitations, Gili et al. proposed an AlGaAs-based monolithic platform for nonlinear nanophotonics, as depicted in Fig. 7(a)[56]. The authors grew their samples by MBE on non-intentionally doped GaAs wafer, with a 400 nm layer of $Al_{0.18}Ga_{0.82}As$ on top of an aluminium-rich layer, to be oxidized at a later stage. After patterning disks by EBL, the samples were dry etched with a non-selective ICP-RIE. Then, the etched samples were oxidized in the oven. After oxidation, each $Al_{0.18}Ga_{0.82}As$ nanocylinder lies upon a uniform AlO_x substrate (see Fig. 7(b)), whose low refractive index (n=1.6) enables sub-wavelength optical confinement in the nanocavity. The authors employed these resonators to study the process of SHG and aimed to understand the effect of the Mie-resonances on the efficiency of the process. A typical power-tuning curve for the SHG from a nanocylinder with a radius of 193 nm is shown in Fig. 7(c).

A similar approach has also been demonstrated by Liu et al, where the authors fabricated a nonlinear metasurface comprised of a square lattice of GaAs nanodisks resonators lying on a low refractive index $(Al_xGa_{1-x})_2O_3$ oxide spacer layer that is formed by selectively oxidizing high-Al content $Al_xGa_{1-x}As$ layers (see Fig. 8)[57]. Figure 8(a) shows the fabrication steps for creating the GaAs metasurfaces starting from molecular beam epitaxial growth of a 300 nm thick layer of $Al_{0.85}Ga_{0.15}As$ followed by a 300 nm thick layer of GaAs on top of a GaAs substrate. A negative tone hydrogen silsesquioxane (HSQ) was used as the mask. The shape of the SiO_x nanodisks was then transferred onto the GaAs and AlGaAs layers using an ICP. Finally, the sample was heated for a selective wet oxidization process that converted the layers of $Al_{0.85}Ga_{0.15}As$ into its oxide $(Al_xGa_{1-x})_2O_3$, which has a low refractive index of n =1.6, see Fig. 8(b). Again, the authors studied the process of SHG from such metasurfaces and tuned the incident wavelength to optimise the SHG conversion efficiency, which peaks at the spectral position of the Mie-resonances, aligned with the maximum of the reflectivity, shown in Fig. 8(c).

Both approaches above for fabricating AlGaAs and GaAs on an insulator, respectively, led to efficiencies that exceed ~10^{-5}. However, in both cases the antennas are sitting on a handle GaAs wafer that is not transparent in the visible range, and therefore limits the nonlinear emission in the forward or backward direction. An important

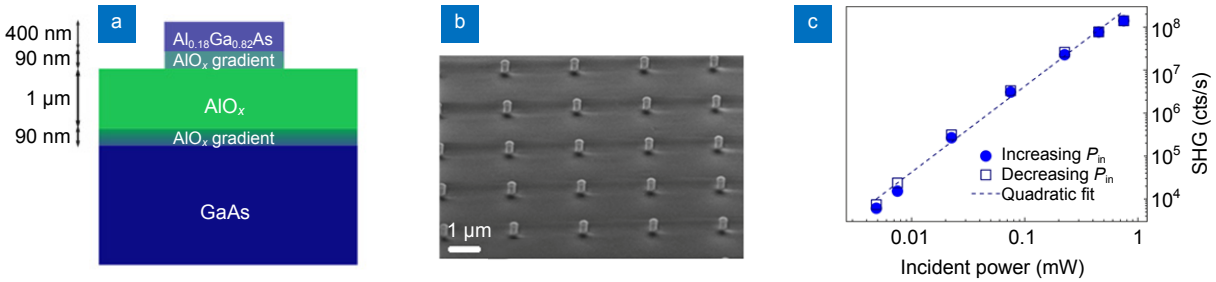

Fig. 7 | (**a**) Schematics of a single Monolithic AlGaAs-on-AlO_x nanoantenna. (**b**) Scanning-electron-microscope picture of a part of the array and (**c**) power curve in Log/Log scale. SHG intensity as a function of the pump intensity for nanoantenna with 193 nm radius. Figure reproduced with permission from ref.[56].

strategy for achieving full control of the harmonic radiation is to be able to fabricate high-quality III-V nanoresonators that can freely emit in both the forward and the backward directions. However, the standard fabrication techniques forbid this approach, as they require a non-transparent III-V substrate for direct growth of III-V semiconductors. The growth on transparent substrates (e.g. glass) is avoided because it results in films with a high density of dislocations. Recently, Camacho et al., have implemented a novel fabrication procedure of AlGaAs-in-insulator, containing epitaxial growth in conjunction with a bonding procedure to a glass substrate[58]. Their final sample contains high-quality $Al_{0.2}Ga_{0.8}As$ nanodisks embedded in a transparent benzocyclobutene (BCB) layer, with an equivalent refractive index to glass, on a glass substrate.

The fabrication steps can be seen in Fig. 9(a). The sample was grown by metalorganic chemical vapour deposition (MOCVD) on a semi-insulating GaAs substrate. First, the 20 nm AlAs buffer layer was grown, followed by 300 nm of an $Al_{0.2}Ga_{0.8}As$ layer. Patterned SiO_x masks were fabricated via standard EBL and subsequently transferred to AlGaAs, AlAs, and GaAs wafer, respectively, by RIE etching. Then, surface treatment was performed via Cl_2 purging, through ICP, to decrease the adhesion between the BCB polymer and the exposed GaAs surface of the wafer. The SiO_x masks and AlAs layers were then removed by hydrofluoric acid, which resulted in minimum adhesion between AlGaAs disks and GaAs wafer. It was followed by spin-coating of 4 μm BCB layer on the sample, then bonding it to a thin glass substrate. Finally, the glass substrate, including the AlGaAs disks embedded

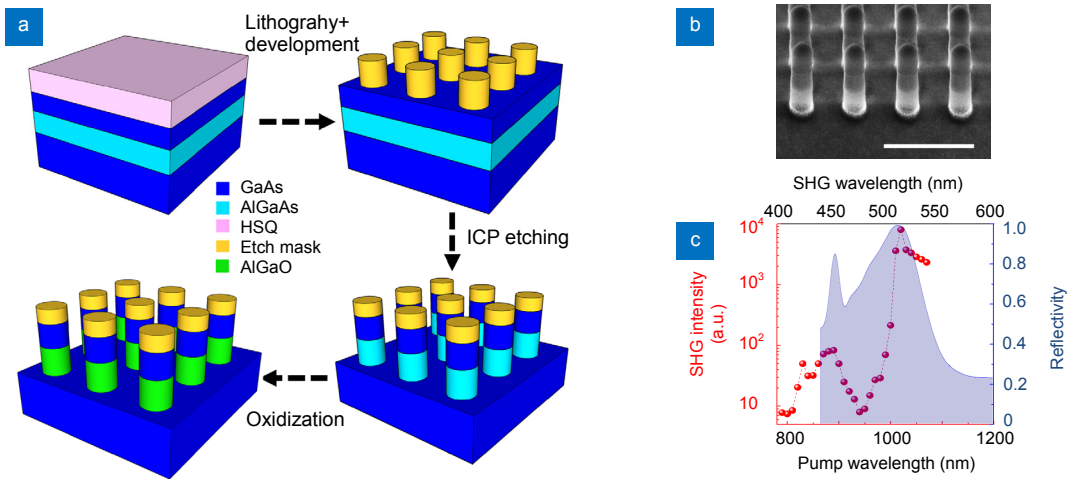

Fig. 8 | (**a**) Steps for fabricating GaAs based dielectric metasurfaces starting with molecular beam epitaxial growth, followed by e-beam lithography patterning, ICP dry etching, and selective wet oxidation. (**b**) A 75° side view. The GaAs resonators have the same diameter of ~250 nm and height of 300 nm. (**c**) The experimental linear reflectivity spectra of the sample are used as the backgrounds. Figure reprinted with permission from ref.[57], American Chemical Society.

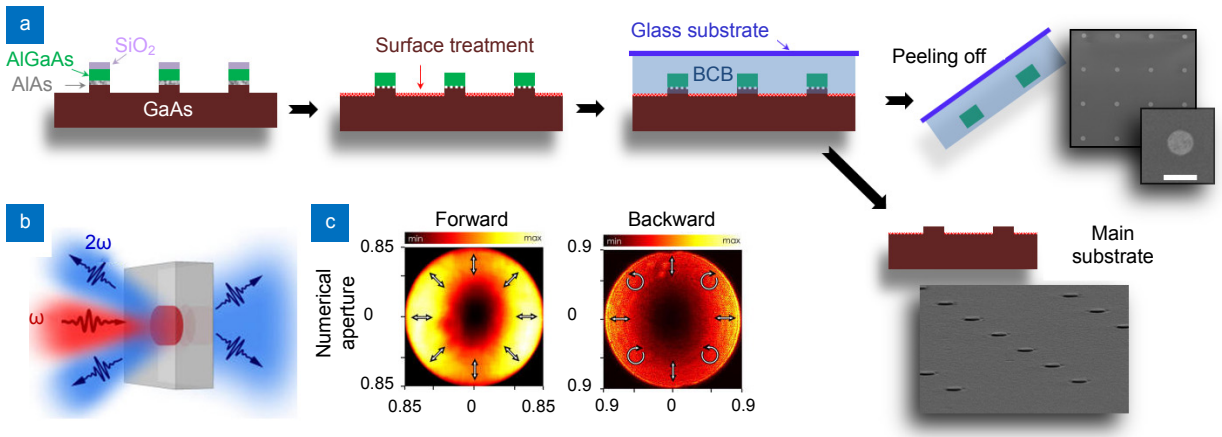

Fig. 9 | (**a**) Steps for fabricating AlGaAs nanoantennas on a glass substrate. (**b**) Schematic of the single antenna experiment in both forward and backward directions. (**c**) Experimentally measured SHG radiation patterns depicting the directionality and polarization diagrams of the SH signal in forward and backward directions. Arrows visualize the polarization states. Figure reprinted with permission from ref.[58], American Chemical Society.

within the BCB layer, was peeled off from the main GaAs wafer[58]. The electron microscopy images of AlGaAs disks and the pillar bases remaining on the original substrate can be seen on the right-hand-side of Fig. 9(a).

This technique allows not only obtaining efficient SHG, but also enabling the control of directionality and full characterisation of the polarization of the nonlinear emission in both forward and backward direction, as shown in Fig. 9(b). Figure 9(c) demonstrates the experimentally measured polarization states in both directions, where vector-beam formation at the SH frequency takes place. Interestingly, in the experiment, one can observe nearly perfect radial polarization of the SH in the forward direction. It is worth mentioning that GaAs family resonators are capable to exhibit nonlinear interaction beyond SHG and THG, e.g. sum-frequency generation, four-wave mixing, etc[81–83]. This is a unique opportunity that enables nonlinear mixing for wide range of applications such as communications and quantum optics.

Hybrid nanoantennas

In the previous sections, it was shown that metallic nanoantennas are a good alternative for nonlinear nanophotonics due to the strong local field enhancement in such systems. Subsequently, it was discussed that high-index dielectric nanoparticles could provide new avenues for the study of nonlinear effects due to their very low losses and large light scattering efficiency. In the meanwhile, some research works have demonstrated that combining the advantages of the metal and dielectric/semiconductor approaches can push the conversion efficiency to even larger values. Various types of hybrid nanoantennas, consisting of metallic resonators embedded in dielectric and semiconductor media or vice-versa, have been proposed and realized in the recent years. Indium tin oxide (ITO) particles within Au nanoantennas[19,20,84–86], is an example of such efforts with promising results. As can be seen in Fig. 10(a), Aouani et al., have obtained a ground breaking 10^6 fold enhancement of THG from an individual ITO nanoparticle, upon being decorated by a gold antenna[20]. Subsequently, there have been several publications, in which the localised fields in nanoscale gaps width of metallic antennas have been studied, through Landau damping[87], hyperbolic cosine catenary function[88], etc.

Similarly, several orders of magnitude increase in nonlinear conversion efficiencies of second- and third-order effects have been demonstrated in plasmonic particles placed on top of nonlinear GaAs substrates[10], nanopatterned plasmonic films filled with GaAs[89], metal/dielectric core-shell nanoparticles[90], plasmonic ring filled by concentric Lithium Niobate[91], silicon[92], AlGaAs[93] disks, etc. It was also shown in linear hybrid nanostructures that plasmonic-Mie mode hybridization can give rise to high radiation directivity[94–96]. The fabrication technique for hybrid nanostructuring is generally a combination of the techniques discussed above, consisting of multiple EBL steps, requiring precise alignment of every subsequent mask to the previous steps.

Layered materials

Layered materials, known as 2D materials and their hetrostructures, are a rapidly growing class of materials with the ability to emit and detect light at different wavelength ranges[97,98]. These materials possess different band gaps and a large range of conductivities. Graphene is the most studied 2D material that has no band gap and behaves like a metal. On the other hand other 2D materials, such as WS_2, MoS_2, $MoSe_2$ and WSe_2 have semiconducting band gaps on the order of 1–2.5 eV, and hexagonal boron nitride (h-BN) with a wide band gap on the order of 6 eV[99]. Very recently, 2D materials have been employed for enhancing nonlinear efficiencies at nanoscale[97]. One of the common issues of 2D materials is that a single monolayer only slightly perturbs the cavity mode. Thus, the cavity is formed by another linear material, while 2D materials only provide the required nonlinearity. For example, by using graphene and hBN layered structures it is possible to create hyperbolic metamaterials[100,101]. Thereby, 2D materials offer an important alternative for enhancing the nonlinear optical interaction[102]. Chemical vapor deposition (CVD) technique is the most employed method

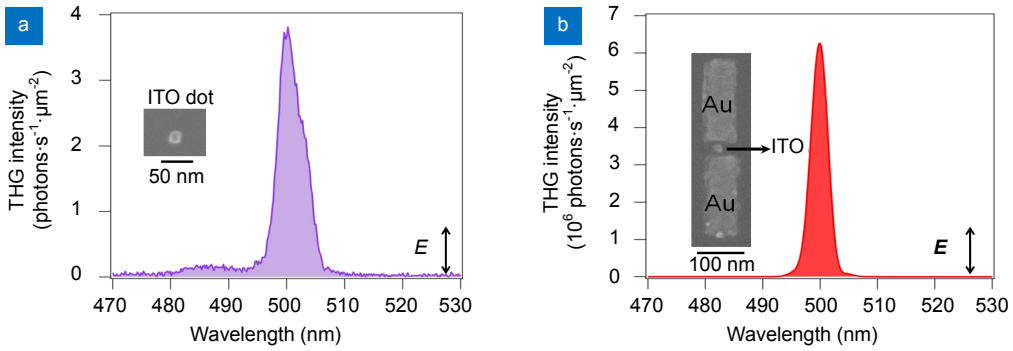

Fig. 10 | Measured THG intensity from (a) an isolated ITO particle (left) versus (b) hybridized ITO-Au antenna. Insets show SEM image of an antenna for each case. Figure reproduced from ref.[20].

that has enabled the synthesis of large area and uniform thickness 2D layer of metal and insulating surfaces for the large-scale device fabrication including electronic and flexible optoelectronic devices[103].

Conclusions

In summary, we have reviewed the area of nonlinear nanoantennas and metasurfaces, including those based on metallic, high-index dielectric, semiconductor, and hybrid nanostructures. We have discussed the role of materials in the harmonic generation, including the relevant fabrication techniques. We explained the evolution of the field, starting with the studying of metallic nanoantennas that are mostly fabricated via standard electron beam lithography and metal evaporation techniques. High-index dielectrics are the second most studied nonlinear nanoantennas that mostly require PECVD for film growth and RIE-ICP for etching. Recently, III-V semiconductors, with large intrinsic second-order nonlinearity, have been the focus of attention. Such nonlinear nanoantennas require either oxidization or transfer techniques. Certainly, the intense current researches in the area of nonlinear nanophotonics are expected to lead to novel industrial applications of nonlinear nanoantennas and metasurfaces, including spectroscopy[7], nanomedicine[104] bio-imaging and sensing[105], generation of coherent ultraviolet light[106], supercontinuum white light generation[107], and quantum optics[108], all within miniaturized nanoscale photonic circuits and miniaturized devices.

References

1. Maiman T H. Stimulated optical radiation in ruby. *Nature* **187**, 493–494 (1960).
2. Boyd R W. *Nonlinear Optics* 2nd ed (Academic Press, Rochester, NY, USA, 2003).
3. Krasnok A, Tymchenko M, Alù A. Nonlinear metasurfaces: A paradigm shift in nonlinear optics. *Mater Today* **21**, 8–21 (2018).
4. Chen L W, Zheng X R, Du Z R, Jia B H, Gu M *et al*. A frozen matrix hybrid optical nonlinear system enhanced by a particle lens. *Nanoscale* **7**, 14982–14988 (2015).
5. Kauranen M, Zayats A V. Nonlinear plasmonics. *Nat Photonics* **6**, 737–748 (2012).
6. Wolf O, Campione S, Benz A, Ravikumar A P, Liu S *et al*. Phased-array sources based on nonlinear metamaterial nanocavities. *Nat Commun* **6**, 7667 (2015).
7. Klein M W, Enkrich C, Wegener M, Linden S. Second-harmonic generation from magnetic metamaterials. *Science* **313**, 502–504 (2006).
8. Aouani H, Navarro-Cia M, Rahmani M, Sidiropoulos T P H, Hong M H *et al*. Multiresonant broadband optical antennas as efficient tunable nanosources of second harmonic light. *Nano Lett* **12**, 4997–5002 (2012).
9. Gennaro S D, Rahmani M, Giannini V, Aouani H, Sidiropoulos T P H *et al*. The interplay of symmetry and scattering phase in second harmonic generation from gold nanoantennas. *Nano Lett* **16**, 5278–5285 (2016).
10. Niesler F B P, Feth N, Linden S, Niegemann J, Gieseler J *et al*. Second-harmonic generation from split-ring resonators on a GaAs substrate. *Opt Lett* **34**, 1997–1999 (2009).
11. Panoiu N C, Sha W E I, Lei D Y, Li G C. Nonlinear optics in plasmonic nanostructures. *J Opt* **20**, 083001 (2018).
12. Midtvedt D, Isacsson A, Croy A. Nonlinear phononics using atomically thin membranes. *Nat Commun* **5**, 4838 (2014).
13. Lee J, Tymchenko M, Argyropoulos C, Chen P Y, Lu F *et al*. Giant nonlinear response from plasmonic metasurfaces coupled to intersubband transitions. *Nature* **511**, 65–69 (2014).
14. Liu H Z, Guo C, Vampa G, Zhang J L, Sarmiento T *et al*. Enhanced high-harmonic generation from an all-dielectric metasurface. *Nat Phys* **14**, 1006–101 (2018).
15. Yang Y M, Wang W Y, Boulesbaa A, Kravchenko I I, Briggs D P *et al*. Nonlinear fano-resonant dielectric metasurfaces. *Nano Lett* **15**, 7388–7393 (2015).
16. Luo X G. Principles of electromagnetic waves in metasurfaces. *Sci China Phys*, *Mech Astron* **58**, 594201 (2015).
17. Hong M H. Metasurface wave in planar nano-photonics. *Sci Bull* **61**, 112–113 (2016).
18. Giannini V, Fernández-Domínguez A I, Heck S C, Maier S A. Plasmonic nanoantennas: Fundamentals and their use in controlling the radiative properties of nanoemitters. *Chem Rev* **111**, 3888–3912 (2011).
19. Metzger B, Hentschel M, Schumacher T, Lippitz M, Ye X C *et al*. Doubling the efficiency of third harmonic generation by positioning ITO nanocrystals into the hot-spot of plasmonic gap-antennas. *Nano Lett* **14**, 2867–2872 (2014).
20. Aouani H, Rahmani M, Navarro-Cía M, Maier S A. Third-harmonic-upconversion enhancement from a single semiconductor nanoparticle coupled to a plasmonic antenna. *Nat Nanotechnol* **9**, 290–294 (2014).
21. Metzger B, Gui L L, Fuchs J, Floess D, Hentschel M *et al*. Strong enhancement of second harmonic emission by plasmonic resonances at the second harmonic wavelength. *Nano Lett* **15**, 3917–3922 (2015).
22. Butet J, Brevet P F, Martin O J F. Optical second harmonic generation in plasmonic nanostructures: From fundamental principles to advanced applications. *ACS Nano* **9**, 10545–10562 (2015).
23. Rahmani M, Shorokhov A S, Hopkins B, Miroshnichenko A E, Shcherbakov M R *et al*. Nonlinear symmetry breaking in symmetric oligomers. *ACS Photonics* **4**, 454–461 (2017).
24. Celebrano M, Wu X F, Baselli M, Großmann S, Biagioni P *et al*. Mode matching in multiresonant plasmonic nanoantennas for enhanced second harmonic generation. *Nat Nanotechnol* **10**, 412–417 (2015).
25. Du Z R, Chen L W, Kao T S, Wu M X, Hong M H. Improved optical limiting performance of laser-ablation-generated metal nanoparticles due to silica-microsphere-induced local field enhancement. *Beilstein J Nanotechnol* **6**, 1199–1204 (2015).
26. Maier S A. *Plasmonics*: *Fundamentals and Applications* (Springer Science & Business Media, New York, 2007).
27. Rahmani M, Tahmasebi T, Lin Y, Lukiyanchuk B, Liew T Y F *et al*. Influence of plasmon destructive interferences on optical properties of gold planar quadrumers. *Nanotechnology* **22**, 245204 (2011).
28. Lu F F, Zhang W D, Huang L G, Liang S H, Mao D *et al*. Mode evolution and nanofocusing of grating-coupled surface plasmon polaritons on metallic tip. *Opto-Electron Adv* **1**, 180010 (2018).
29. Chen L W, Zhou Y, Wu M X, Hong M H. Remote-mode microsphere nano-imaging: new boundaries for optical microscopes.

Opto-Electron Adv **1**, 170001 (2018).
30. Rahmani M, Luk'yanchuk B, Hong M H. Fano resonance in novel plasmonic nanostructures. *Laser Photonics Rev* **7**, 329–349 (2013).
31. Zhang W Q, Rahmani M, Niu W X, Ravaine S, Hong M H *et al*. Tuning interior nanogaps of double-shelled Au/Ag nanoboxes for surface-enhanced raman scattering. *Sci Rep* **5**, 8382 (2015).
32. Della Picca F, Berte R, Rahmani M, Albella P, Bujjamer J M *et al*. Tailored hypersound generation in single plasmonic nanoantennas. *Nano Lett* **16**, 1428–1434 (2016).
33. Kuznetsov A I, Miroshnichenko A E, Fu Y H, Viswanathan V, Rahmani M *et al*. Split-ball resonator as a three-dimensional analogue of planar split-rings. *Nat Commun* **5**, 3104 (2014).
34. Hanke T, Cesar J, Knittel V, Trügler A, Hohenester U *et al*. Tailoring spatiotemporal light confinement in single plasmonic nanoantennas. *Nano Lett* **12**, 992–996 (2012).
35. Fernandez-Garcia R, Rahmani M, Hong M H, Maier S A, Sonnefraud Y. Use of a gold reflecting-layer in optical antenna substrates for increase of photoluminescence enhancement. *Opt Express* **21**, 12552–12561 (2013).
36. Yoxall E, Navarro-Cía M, Rahmani M, Maier S A, Phillips C C. Widely tuneable scattering-type scanning near-field optical microscopy using pulsed quantum cascade lasers. *Appl Phys Lett* **103**, 213110 (2013).
37. Geraci G, Hopkins B, Miroshnichenko A E, Erkihun B, Neshev D N *et al*. Polarisation-independent enhanced scattering by tailoring asymmetric plasmonic systems. *Nanoscale* **8**, 6021–6027 (2016).
38. Rifat A A, Rahmani M, Xu L, Miroshnichenko A E. Hybrid metasurface based tunable near-perfect absorber and plasmonic sensor. *Materials* **11**, 1091 (2018).
39. Franken P, Hill A E, Peters C W, Weinreich G. Generation of optical harmonics. *Phys Rev Lett* **7**, 118–119 (1961).
40. Segovia P, Marino G, Krasavin A V, Olivier N, Wurtz G A *et al*. Hyperbolic metamaterial antenna for second-harmonic generation tomography. *Opt Express* **23**, 30730–30738 (2015).
41. Marino G, Segovia P, Krasavin A V, Ginzburg P, Olivier N *et al*. Second-harmonic generation from hyperbolic plasmonic nanorod metamaterial slab. *Laser Photonics Rev* **12**, 1700189 (2018).
42. Wang P, Krasavin A V, Nasir M E, Dickson W, Zayats A V. Reactive tunnel junctions in electrically driven plasmonic nanorod metamaterials. *Nat Nanotechnol* **13**, 159–164 (2018).
43. Dickson W, Beckett S, McClatchey C, Murphy A, O'Connor D *et al*. Hyperbolic polaritonic crystals based on nanostructured nanorod metamaterials. *Adv Mater* **27**, 5974–5980 (2015).
44. Shorokhov A S, Melik-Gaykazyan E V, Smirnova D A, Hopkins B, Chong K E *et al*. Multifold enhancement of third-harmonic generation in dielectric nanoparticles driven by magnetic fano resonances. *Nano Lett* **16**, 4857–4861 (2016).
45. Grinblat G, Li Y, Nielsen M P, Oulton R F, Maier S A. Enhanced third harmonic generation in single germanium nanodisks excited at the anapole mode. *Nano Lett* **16**, 4635–4640 (2016).
46. Nielsen M P, Lafone L, Rakovich A, Sidiropoulos T P H, Rahmani M *et al*. Adiabatic nanofocusing in hybrid gap plasmon waveguides on the silicon-on-insulator platform. *Nano Lett* **16**, 1410–1414 (2016).
47. Caldarola M, Albella P, Cortés E, Rahmani M, Roschuk T *et al*. Non-plasmonic nanoantennas for surface enhanced spectroscopies with ultra-low heat conversion. *Nat Commun* **6**, 7915 (2015).
48. Ikeda K, Shen Y M, Fainman Y. Enhanced optical nonlinearity in amorphous silicon and its application to waveguide devices. *Opt Express* **15**, 17761–17771 (2007).
49. Gai X, Choi D Y, Luther-Davies B. Negligible nonlinear absorption in hydrogenated amorphous silicon at 1.55 μm for ultra-fast nonlinear signal processing. *Opt Express* **22**, 9948–9958 (2014).
50. Fauchet P M, Hulin D. Ultrafast carrier relaxation in hydrogenated amorphous silicon. *J Opt Sci Am B* **6**, 1024–1029 (1989).
51. Sheik-Bahae M, Said A A, Wei T H, Hagan D J, Van Stryland E W. Sensitive measurement of optical nonlinearities using a single beam. *IEEE J of Quantum Electron* **26**, 760–769 (1990).
52. Boyd G D, Patel C K N. Enhancement of optical second‐harmonic generation (SHG) by reflection phase matching in Zns and GaAs. *Appl Phys Lett* **8**, 313–315 (1966).
53. Carletti L, Locatelli A, Stepanenko O, Leo G, De Angelis C. Enhanced second-harmonic generation from magnetic resonance in ALGaAs nanoantennas. *Opt Express* **23**, 26544–26550 (2015).
54. Cambiasso J, Grinblat G, Li Y, Rakovich A, Cortés E *et al*. Bridging the gap between dielectric nanophotonics and the visible regime with effectively lossless gallium phosphide antennas. *Nano Lett* **17**, 1219–1225 (2017).
55. Person S, Jain M, Lapin Z, Sáenz J J, Wicks G *et al*. Demonstration of zero optical backscattering from single nanoparticles. *Nano Lett* **13**, 1806–1809 (2013).
56. Gili V F, Carletti L, Locatelli A, Rocco D, Finazzi M *et al*. Monolithic ALGaAs second-harmonic nanoantennas. *Opt Express* **24**, 15965–15971 (2016).
57. Liu S, Sinclair M B, Saravi S, Keeler G A, Yang Y M *et al*. Resonantly enhanced second-harmonic generation using III–V semiconductor all-dielectric metasurfaces. *Nano Lett* **16**, 5426–5432 (2016).
58. Camacho-Morales R, Rahmani M, Kruk S, Wang L, Xu L *et al*. Nonlinear generation of vector beams from ALGaAs nanoantennas. *Nano Lett* **16**, 7191–7197 (2016).
59. Shcherbakov M R, Shorokhov A S, Neshev D N, Hopkins B, Staude I *et al*. Nonlinear interference and tailorable third-harmonic generation from dielectric oligomers. *ACS Photonics* **2**, 578–582 (2015).
60. Della Valle G, Hopkins B, Ganzer L, Stoll T, Rahmani M *et al*. Nonlinear anisotropic dielectric metasurfaces for ultrafast nanophotonics. *ACS Photonics* **4**, 2129–2136 (2017).
61. Chen S M, Rahmani M, Li K F, Miroshnichenko A, Zentgraf T *et al*. Third harmonic generation enhanced by multipolar interference in complementary silicon metasurfaces. *ACS Photonics* **5**, 1671–1675 (2018).
62. Nemati A, Wang Q, Hong M H, Teng J H. Tunable and reconfigurable metasurfaces and metadevices. *Opto-Electron Adv* **1**, 180009 (2018).
63. Grinblat G, Li Y, Nielsen M P, Oulton R F, Maier S A. Degenerate four-wave mixing in a multiresonant germanium nanodisk. *ACS Photonics* **4**, 2144–2149 (2017).
64. Chen L M, Jiang X F, Guo Z M, Zhu H, Kao T S *et al*. Tuning optical nonlinearity of laser-ablation-synthesized silicon nanoparticles via doping concentration. *J Nanomater* **2014**, 652829 (2014).
65. Wang L, Kruk S, Xu L, Rahmani M, Smirnova D *et al*. Shaping the third-harmonic radiation from silicon nanodimers. *Nanoscale* **9**, 2201–2206 (2017).
66. Makarov S V, Petrov M I, Zywietz U, Milichko V, Zuev D *et al*.

Efficient second-harmonic generation in nanocrystalline silicon nanoparticles. *Nano Lett* **17**, 3047–3053 (2017).
67. Melik-Gaykazyan E V, Kruk S S, Camacho-Morales R, Xu L, Rahmani M *et al*. Selective third-harmonic generation by structured light in mie-resonant nanoparticles. *ACS Photonics* **5**, 728–733 (2018).
68. Tong W Y, Gong C, Liu X J, Yuan S, Huang Q Z *et al*. Enhanced third harmonic generation in a silicon metasurface using trapped mode. *Opt Express* **24**, 19661–19670 (2016).
69. Kuznetsov A I, Miroshnichenko A E, Fu Y H, Zhang J B, Luk'yanchuk B. Magnetic light. *Sci Rep* **2**, 492 (2012).
70. Smirnova D, Kivshar Y S. Multipolar nonlinear nanophotonics. *Optica* **3**, 1241–1255 (2016).
71. Lu B H, Lan H B, Liu H Z. Additive manufacturing frontier: 3D printing electronics. *Opto-Electron Adv* **1**, 170004 (2018).
72. Shcherbakov M R, Neshev D N, Hopkins B, Shorokhov A S, Staude I *et al*. Enhanced third-harmonic generation in silicon nanoparticles driven by magnetic response. *Nano Lett* **14**, 6488–6492 (2014).
73. Choi W K, Liew T H, Dawood M K, Smith H I, Thompson C V *et al*. Synthesis of silicon nanowires and nanofin arrays using interference lithography and catalytic etching. *Nano Lett* **8**, 3799–3802 (2008).
74. Rahmani M, Xu L, Miroshnichenko A E, Komar A, Camacho-Morales R *et al*. Reversible thermal tuning of all-dielectric metasurfaces. *Adv Funct Mater* **27**, 1700580 (2017).
75. Shcherbakov M R, Vabishchevich P P, Shorokhov A S, Chong K E, Choi D Y *et al*. Ultrafast all-optical switching with magnetic resonances in nonlinear dielectric nanostructures. *Nano Lett* **15**, 6985–6990 (2015).
76. Xu L, Rahmani M, Kamali K Z, Lamprianidis A, Ghirardini L *et al*. Boosting third-harmonic generation by a mirror-enhanced anapole resonator. *Light*: *Sci Appl* **7**, 44 (2018).
77. Löchner F J, Fedotova A N, Liu S, Keeler G A, Peake G M *et al*. Polarization-dependent second harmonic diffraction from resonant gaas metasurfaces. *ACS Photonics* **5**, 1786–1793 (2018).
78. Mie G. Beiträge zur optik trüber medien, speziell kolloidaler metallösungen. *Ann Phys* **330**, 377–445 (1908).
79. Debye P. Der lichtdruck auf kugeln von beliebigem material. *Ann Phys* **335**, 57–136 (1909).
80. Xu L, Rahmani M, Smirnova D, Zangeneh Kamali K, Zhang G Q *et al*. Highly-efficient longitudinal second-harmonic generation from doubly-resonant algaas nanoantennas. *Photonics* **5**, 29 (2018).
81. Liu S, Vabishchevich P P, Vaskin A, Reno J L, Keeler G A *et al*. An all-dielectric metasurface as a broadband optical frequency mixer. *Nat Commun* **9**, 2507 (2018).
82. Carletti L, Marino G, Ghirardini L, Gili V F, Rocco D *et al*. Nonlinear goniometry by second-harmonic generation in algaas nanoantennas. *ACS Photonics* **5**, 4386–4392 (2018).
83. Shcherbakov M R, Liu S, Zubyuk V V, Vaskin A, Vabishchevich P P *et al*. Ultrafast all-optical tuning of direct-gap semiconductor metasurfaces. *Nat Commun* **8**, 17 (2017).
84. Aouani H, Navarro-Cía M, Rahmani M, Maier S A. Unveiling the origin of third harmonic generation in hybrid ITO–plasmonic crystals. *Adv Opt Mater* **3**, 1059–1065 (2015).
85. Linnenbank H, Grynko Y, Förstner J, Linden S. Second harmonic generation spectroscopy on hybrid plasmonic/dielectric nanoantennas. *Light*: *Sci Appl* **5**, e16013 (2016).
86. Abb M, Albella P, Aizpurua J, Muskens O. All-optical control of a single plasmonic nanoantenna–ITO hybrid. *Nano Lett* **11**, 2457–2463 (2011).
87. Khurgin J, Tsai W Y, Tsai D P, Sun G. Landau damping and limit to field confinement and enhancement in plasmonic dimers. *ACS Photonics* **4**, 2871–2880 (2017).
88. Pu M B, Guo Y H, Li X, Ma X L, Luo X G. Revisitation of extraordinary young's interference: From catenary optical fields to spin-orbit interaction in metasurfaces. *ACS Photonics* **5**, 3198–3204 (2018).
89. Fan W J, Zhang S, Panoiu N C, Abdenour A, Krishna S *et al*. Second harmonic generation from a nanopatterned isotropic nonlinear material. *Nano Lett* **6**, 1027–1030 (2006).
90. Pu Y, Grange R, Hsieh C L, Psaltis D. Nonlinear optical properties of core-shell nanocavities for enhanced second-harmonic generation. *Phys Rev Lett* **104**, 207402 (2010).
91. Lehr D, Reinhold J, Thiele I, Hartung H, Dietrich K *et al*. Enhancing second harmonic generation in gold nanoring resonators filled with lithium niobate. *Nano Lett* **15**, 1025–1030 (2015).
92. Shibanuma T, Grinblat G, Albella P, Maier S A. Efficient third harmonic generation from metal–dielectric hybrid nanoantennas. *Nano Lett* **17**, 2647–2651 (2017).
93. Gili V F, Ghirardini L, Rocco D, Marino G, Favero I *et al*. Metal–dielectric hybrid nanoantennas for efficient frequency conversion at the anapole mode. *Beilstein J Nanotechnol* **9**, 2306–2314 (2018).
94. Decker M, Pertsch T, Staude I. Strong coupling in hybrid metal–dielectric nanoresonators. *Philos Trans Roy Soc A*: *Math*, *Phys Eng Sci* **375**, 20160312 (2017).
95. Guo R, Rusak E, Staude I, Dominguez J, Decker M *et al*. Multipolar coupling in hybrid metal–dielectric metasurfaces. *ACS Photonics* **3**, 349–353 (2016).
96. Rusak E, Staude I, Decker M, Sautter J, Miroshnichenko A E *et al*. Hybrid nanoantennas for directional emission enhancement. *Appl Phys Lett* **105**, 221109 (2014).
97. Xia F N, Wang H, Xiao D, Dubey M, Ramasubramaniam A. Two-dimensional material nanophotonics. *Nat Photonics* **8**, 899 (2014).
98. Zheng X R, Jia B H, Chen X, Gu M. In situ third-order non-linear responses during laser reduction of graphene oxide thin films towards on-chip non-linear photonic devices. *Adv Mater* **26**, 2699–2703 (2014).
99. Fryett T, Zhan A, Majumdar A. Cavity nonlinear optics with layered materials. *Nanophotonics* **7**, 69 (2017).
100. Dai S, Ma Q, Liu M K, Andersen T, Fei Z *et al*. Graphene on hexagonal boron nitride as a tunable hyperbolic metamaterial. *Nat Nanotechnol* **10**, 682–686 (2015).
101. Kumar A, Low T, Fung K H, Avouris P, Fang N X. Tunable light–matter interaction and the role of hyperbolicity in graphene–hbn system. *Nano Lett* **15**, 3172–3180 (2015).
102. Poddubny A, Iorsh I, Belov P, Kivshar Y. Hyperbolic metamaterials. *Nat Photonics* **7**, 948–957 (2013).
103. Gupta A, Sakthivel T, Seal S. Recent development in 2D materials beyond graphene. *Prog Mater Sci* **73**, 44–126 (2015).
104. Geissbuehler M, Bonacina L, Shcheslavskiy V, Bocchio N L, Geissbuehler S *et al*. Nonlinear correlation spectroscopy (NLCS). *Nano Lett* **12**, 1668–1672 (2012).
105. DaCosta M V, Doughan S, Han Y, Krull U J. Lanthanide upconversion nanoparticles and applications in bioassays and bioimaging: A review. *Anal Chim Acta* **832**, 1–33 (2014).
106. Makarov S V, Tsypkin A N, Voytova T A, Milichko V A, Mukhin I S *et al*. Self-adjusted all-dielectric metasurfaces for deep ultraviolet femtosecond pulse generation. *Nanoscale* **8**, 17809–17814

(2016).

107. Krasavin A V, Ginzburg P, Wurtz G A, Zayats A V. Nonlocality-driven supercontinuum white light generation in plasmonic nanostructures. *Nat Commun* **7**, 11497 (2016).
108. Barz S, Cronenberg G, Zeilinger A, Walther P. Heralded generation of entangled photon pairs. *Nat Photonics* **4**, 553–556 (2010).

Acknowledgements

The authors acknowledge the financial support provided by the Australian Research Council (ARC) and participation in the Erasmus Mundus NANOPHI project, contract number 2013 5659/002-001. M. R. sincerely appreciates funding from an ARC Discovery Early Career Research Fellowship (DE170100250) and funding from the Australian Nanotechnology Network. M. R. and A. E. M. appreciate a funding from Australia–Germany Joint Research Cooperation Scheme. The work of A. E. M. was supported by a UNSW Scientia Fellowship. G. L. and V. F. G. acknowledge funding from SEAM Labex (PANAMA project)". A. V. Z., S. A. M. and R.O. acknowledge the funding provided by the EPSRC Reactive Plasmonics Programme (EP/M013812/1), the ONR Global, the Leverhulme Trust, the Royal Society (UF150542). A. V. Z. acknowledges support from the Royal Society and the Wolfson Foundation. S. A. M. appreciates supports from the Lee-Lucas Chair in Physics and acknowledges the DFG Cluster of Excellence Nanoinitiative Munich (NIM), and the Solar Technologies Go Hybrid (SOLTEC) projects. I. S. gratefully acknowledges financial support by the German Research Foundation (STA 1426/2-1) and the Thuringian State Government within its ProExcellence initiative (APC^{2020}). I. B. acknowledges the support of the U.S. Department of Energy, Office of Basic Energy Sciences, Division of Materials Sciences and Engineering. I. B., I. S. and D. N. N. acknowledge the support of the Center for Integrated Nanotechnologies, an Office of Science User Facility operated for the U.S. Department of Energy (DOE) Office of Science. Sandia National Laboratories is a multi-mission laboratory managed and operated by National Technology and Engineering Solutions of Sandia, LLC, a wholly owned subsidiary of Honeywell International, Inc., for the U.S. Department of Energy's National Nuclear Security Administration under contract DE-NA0003525. This paper describes objective technical results and analysis. Any subjective views or opinions that might be expressed in the paper do not necessarily represent the views of the U.S. Department of Energy or the United States Government. The authors acknowledge the use of the Australian National Fabrication Facility (ANFF), the ACT Node.

Competing interests

The authors declare no competing financial interests.